

Reconciling *Planck* cluster counts and cosmology: *Chandra/XMM* instrumental calibration and hydrostatic mass bias

Holger Israel^{1,*}, Gerrit Schellenberger², Jukka Nevalainen³,

Richard J. Massey¹, and Thomas H. Reiprich²

¹*Institute for Computational Cosmology, Department of Physics, Durham University, South Road, Durham DH1 3LE, UK*

²*Argelander-Institut für Astronomie, Auf dem Hügel 71, 53121 Bonn, Germany*

³*Tartu Observatory, 61602 Toravere, Estonia*

**E-mail: holger.israel@durham.ac.uk*

6 December 2024

ABSTRACT

The temperature of X-ray emitting gas T_X is often used to infer the total mass of galaxy clusters (under the assumption of hydrostatic equilibrium). Unfortunately, *XMM-Newton* and *Chandra* observatories measure inconsistent temperatures for the same gas, due to uncertain instrumental calibration. We translate the relative bias in temperature measurements of Schellenberger et al. (2014) into a bias on inferred mass for a sample of clusters with homogeneous weak lensing (WL) masses, in order to simultaneously examine the hydrostatic bias and instrument calibration. Israel et al. (2014) found consistent WL and *Chandra* hydrostatic X-ray masses for a sample of clusters at $z \sim 0.5$ and masses of a few $10^{14} M_\odot$. Re-evaluating the latter, we find their *XMM-Newton* masses to be lower by $b^{\text{cal}} = 15\text{--}20\%$ than their *Chandra* masses. At the massive end ($\gtrsim 5 \cdot 10^{14} M_\odot$), the *XMM-Newton* masses are $\sim 35\%$ lower than the WL masses. Assuming that the true hydrostatic bias is 20 %, as indicated by simulations, our results for the massive end indicate that *Chandra*'s calibration of the energy dependence of the effective area is more accurate than *XMM-Newton*'s. However, the opposite appears to be true at the low mass end, unless the hydrostatic bias vanishes there, although larger samples are required to firmly establish this trend.

In addition, we follow through how a bias in the T_X would affect the *Planck* cluster counts. X-ray masses feature prominently in the apparent discrepancy between *Planck* measurements of the primary Cosmic Microwave Background (CMB) and the number of clusters detected via the Sunyaev-Zeldovich (SZ) effect. The SZ masses were indirectly calibrated via *XMM-Newton* observations. Assuming the *Chandra* calibration to be correct, an amplified residual calibration bias (up to $\sim 30\%$ in mass) could ease the tension in the cosmological interpretation, while keeping the bias due to departures from hydrostatic equilibrium $b^{\text{hyd}} \sim 0.2$, as expected from simulations.

Key words: Galaxies: clusters: general – Cosmology: observations – Gravitational lensing – X-rays: galaxies: clusters

1 INTRODUCTION

The number count of Sunyaev-Zeldovich (SZ) clusters measured with *Planck* to lie above a certain mass threshold (Planck Collaboration et al. 2013c, P13XX) falls short of the tally expected from the *Planck* primary cosmic microwave background (CMB) constraints on cosmology (Planck Collaboration et al. 2013b, P13XVI). Several possible explanations have been brought forward, such as incorrect assumptions about the cluster mass function (P13XX) or modi-

fied cosmologies including massive neutrinos and a shift in the Hubble parameter (e.g., P13XX, Hamann & Hasenkamp 2013; Battye & Moss 2014; Mantz et al. 2014; Costanzi et al. 2014). Another hypothesis is that hydrostatic cluster masses, inferred from X-ray analyses of the intra-cluster medium (ICM), yielded only $\sim 60\%$ of the true cluster mass. Hydrodynamic cluster simulations commonly find the hydrostatic assumption to retrieve only $\sim 70\text{--}90\%$ of the true cluster mass, i.e. $M^{\text{HE}} = (1 - b_{\text{lin}}^{\text{hyd}})M^{\text{true}}$ with a hydrostatic mass bias $b_{\text{lin}}^{\text{hyd}} = 0.1\text{--}0.3$ (e.g., Nagai, Kravtsov & Vikhlinin 2007;

Laganá, de Souza & Keller 2010; Kay et al. 2012; Rasia et al. 2012; Le Brun et al. 2014; Schaye et al. 2014). However, hydrostatic masses are subject to systematic uncertainties stemming from, e.g., the finite accuracy of the calibration of the effective area (i.e. cluster temperature), which is known to vary significantly between X-ray instruments (e.g. Nevalainen, David & Guainazzi 2010). In this article, we re-evaluate the Israel et al. (2014, I14) measurement of the mass bias between *Chandra* hydrostatic and weak lensing masses for a sample of X-ray-selected clusters. We emulate *XMM-Newton* results based on the correspondence between ICM temperatures T_X measured with the two observatories that was recently established by Schellenberger et al. (2014, S14). Noticing that the P13XX calibration relies on *XMM-Newton*, we thus assess the role the X-ray temperature calibration plays concerning the P13XX–P13XVI discrepancy.

1.1 What did the *Planck* collaboration measure?

P13XX model the redshift-dependent abundance of clusters detected from the *Planck* catalogue of Sunyaev-Zeldovich sources (Planck Collaboration et al. 2013a, P13XXIX), covering the whole extragalactic sky. The thermal SZ effect describes the inverse Compton scattering of CMB photons with ICM electrons, resulting in a distortion Y_{SZ} of the CMB signal in the solid angle subtended by a galaxy cluster, proportional to the integrated electron pressure. All 189 $S/N > 7$ sources selected from the P13XXIX catalogue are confirmed clusters of known redshift; the vast majority with spectroscopic redshifts. The P13XXIX mass estimates M^{Pl} ($M^{Y_{\text{SZ}}}$ in P13XXIX) that enter the P13XX calculation are the only, and crucial, piece of *Planck* data P13XX use.

Due to the large beam compared to the typical *Planck* cluster size, the aperture size θ , in which Y_{SZ} is integrated, is hard to determine from the SZ data itself. P13XXIX rely on the additional $Y_{\text{SZ}}(\theta)$ constraint provided by the scaling of Y_{SZ} with an X-ray mass proxy, $M_{500}^{Y_X}$, to fix θ and calibrate the M^{Pl} . By convention, r_{Δ} denotes a radius such that the mass M_{Δ} within it exceeds the critical density $\rho_c(z)$ at redshift z by a factor of Δ . The $M_{500}^{Y_X}$ mass proxy is based on $Y_X = T_X M_{\text{gas}}$, which is the product of the ICM temperature T_X and the cluster gas mass M_{gas} , measured from X-rays within r_{500} , and thus provides an X-ray analogue of Y_{SZ} .¹

P13XX calibrate M^{Pl} on a validation sub-sample of 71 clusters observed with *XMM-Newton*, i.e. they derive the best-fit $Y_{\text{SZ},500} - M_{500}^{Y_X}$ relation. In turn, $M_{500}^{Y_X}$ was calibrated on a sample of local, relaxed clusters whose “true” masses could be measured using X-ray observations and assuming hydrostatic equilibrium (Arnaud et al. 2010). It is via this ladder of mass proxies that the hydrostatic mass bias is inherited onto M^{Pl} , appearing in the $Y_{\text{SZ},500} - M_{500}^{Y_X}$ relation that summarises the calibration process (Eq. A.8 of P13XX). P13XX considered a flat prior of $0.7 < (1 - b_{\text{lin}}) < 1$, but any additional systematic effect in the calibration chain would mimic a spurious “hydrostatic” bias.

¹ The accuracy in M_{gas} depends on the accuracy of the calibration effective area normalisation, i.e. the calibration of the flux S . As $M_{\text{gas}} \propto \sqrt{S}$, the maximal flux difference in Nevalainen, David & Guainazzi (2010) of 10 % corresponds to 5 % uncertainty in M_{gas} . This is relatively small; so we ignore it and focus on T_X .

1.2 What do weak lensing surveys measure?

Weak gravitational lensing (WL) provides an avenue to determine cluster masses M^{wl} that is independent of the assumption of hydrostatic equilibrium. Noticing a considerable overlap between the *XMM-Newton* sample of P13XX and the *Weighing the Giants* WL survey (von der Linden et al. 2014a; Kelly et al. 2014; Applegate et al. 2014), von der Linden et al. (2014b, vdL14) measured $\langle M^{\text{Pl}}/M^{\text{wl}} \rangle = 0.688 \pm 0.072$ for the most massive ($> 6 \cdot 10^{14} M_{\odot}$) clusters. This is consistent with our results (see Sect. 3.1). If interpreted as a hydrostatic mass bias, this value falls between the $b_{\text{lin}} \approx 0.2$ favoured by simulations and the $b_{\text{lin}} \approx 0.4$ necessary to reconcile P13XX with P13XVI. While their results confirm the *Planck* cluster mass discrepancy, vdL14 suggest that biases in the *XMM-Newton* temperature calibration contribute to the *Planck* discrepancy.

However, Israel et al. (2014, I14) found no significant mass bias when gauging *Chandra*-based hydrostatic masses for their clusters with WL mass estimates. For the whole mass range of $10^{14} M_{\odot} < M_{500}^{\text{wl}} < 10^{15} M_{\odot}$, the bias vanishes: $b_{\text{log}} = \langle \log M_{500}^{\text{HE}} - \log M_{500}^{\text{wl}} \rangle = 0.00^{+0.14}_{-0.13}$. The high-mass half-sample ($10^{14.5} M_{\odot} < M_{500}^{\text{wl}} < 10^{15} M_{\odot}$) yields a bias of $b_{\text{log}} = -0.10^{+0.17}_{-0.15}$, consistent with the expectation based on simulations, although with large uncertainties due to the small number statistics. Here, we set out to examine simultaneously the hydrostatic bias and the *XMM-Newton*/*Chandra* temperature calibration.

1.3 On X-ray temperature cross-calibration

Measurements of T_X from satellite observatories are subject to uncertainties in the instrumental calibration, mainly due to the difficulty of modelling accurately their energy-dependent effective collecting area. The International Astronomical Consortium for High Energy Calibration (IACHEC) has tasked itself with improving (cross-)calibrations of X-ray satellite observatories (Grant et al. 2013). In this context, Schellenberger et al. (2014, S14) published a detailed comparison of *Chandra* and *XMM-Newton* temperatures for HI-FLUGCS, a statistically complete sample of 64 high-flux local clusters, fitting spectra in the same radial and energy ranges. S14 not only confirmed earlier studies (e.g. Nevalainen, David & Guainazzi 2010) that *Chandra* yields significantly higher T_X than *XMM-Newton*, but also find significant differences between the *XMM-Newton* instruments. These temperature differences are most pronounced at the highest plasma temperatures and can best be explained as effective area calibration uncertainties, as S14 demonstrate.

Moreover, S14 quantified the effect of measuring *XMM-Newton* masses, scaled individually for each cluster from *Chandra*, on the cosmic matter density Ω_m and power spectrum normalisation σ_8 . S14 find the shift of uncertainty ellipses in the $\sigma_8 - \Omega_m$ plane due to the temperature calibration insufficient to explain the offset of such contours between P13XVI and P13XX. We extend this work by comparisons with WL masses and thus aim at simultaneously examining the hydrostatic bias and instrument calibration to find a solution for the cosmology problem.

2 RECALIBRATING THE 400D SURVEY TO XMM-NEWTON TEMPERATURES

2.1 Hydrostatic mass bias from the 400d cluster cosmology survey

I14 recently compared WL masses to *Chandra*-based X-ray mass estimates for eight clusters drawn from the 400d cosmology cluster sample. The 400d cosmology sample selects X-ray luminous clusters at $0.35 < z < 0.90$ from the serendipitous 400d *Rosat* cluster catalogue (Burenin et al. 2007). *Chandra* data for these clusters were subsequently employed to constrain cosmological parameters via the cluster mass function (Vikhlinin et al. 2009a,b). The 400d WL survey follows up the cosmology cluster sample, in order to test the mass calibration of V09a,b with independent mass estimates. The methodology and first results of the ongoing 400d WL survey were reported in Israel et al. (2010, 2012). We refer the interested reader to these papers for details. Weak lensing masses used in this paper make use of the Bhattacharya et al. (2013) mass-concentration relation.

Hydrostatic masses in I14 were derived from the V09a *Chandra* ICM density profiles ρ_g using the Vikhlinin et al. (2006) parametrisation, and temperatures $T_X(r) = T_{\text{CXO}}(r)$. The empirical Reiprich et al. (2013) relation was used to derive a temperature profile

$$T_X(r) = T_X (1.19 - 0.84r/r_{200}) \quad (1)$$

from a cluster-averaged value T_X and I14 WL radius r_{200} . This relation was determined and can be used in the range $0.3r_{200} < r < 1.15r_{200}$. We then compute

$$M^{\text{HE}}(r) = \frac{-k_B T_X(r) r}{\mu m_p G} \left(\frac{d \ln \rho_g(r)}{d \ln r} + \frac{d \ln T_X(r)}{d \ln r} \right), \quad (2)$$

with k_B the Boltzmann constant, $\mu = 0.5954$ the mean molecular mass of the ICM, m_p the proton mass, and G the gravitational constant. The resulting cumulative mass profile was evaluated at r_{500} taken from WL. Uncertainties on T_{CXO} and r_{500}^{wl} were propagated into an uncertainty on $M_{500}^{\text{hyd}}(r_{500}^{\text{wl}})$.

2.2 Pseudo-XMM-Newton temperatures for the 400d clusters

We translate the ICM temperatures T_{CXO} measured for the 400d clusters with *Chandra* to pseudo-XMM-Newton temperatures by applying the S14 conversion formula between ACIS and the combined *XMM-Newton* instruments for the full spectral energy range:

$$\log \left(\frac{k_B T_{\text{XMM}}}{1 \text{ keV}} \right) = A \cdot \log \left(\frac{k_B T_{\text{CXO}}}{1 \text{ keV}} \right) + B, \quad (3)$$

with $A = 0.889 \pm 0.004$ and $B = 0.016 \pm 0.004$. By applying this conversion, we emulate what ICM temperatures would have been obtained for the 400d clusters, had they been inferred from both the Metal Oxide Semi-conductor (MOS) and the pn-CCD (PN) instruments (collectively, the *XMM-Newton European Photon Imaging Camera*, EPIC) instead of *Chandra*'s Advanced CCD Imaging Spectrometer (ACIS).

Both the calibration of an X-ray instrument and our knowledge about it evolve with time. S14 assume calibrations as of December 2012 (*Chandra* Calibration Database v4.2), while V09a used the unchanged Vikhlinin et al. (2005)

calibration procedure. This is a no Calibration Database calibration, but at the time of observation v3.1 was in place. Using the timestamp correction of ICM temperatures between different Calibration Databases (Reese et al. 2010), we convert the V09a temperatures to the one used by S14 (version 4.2). From Eq. (23) of Reese et al. (2010), we take a factor of $T_{\text{CXO},3.1}/T_{\text{CXO},4.2} = 1.06 \pm 0.05$. We point out that we do not apply the timestamp correction to the T_{CXO} , but rather its inverse to the XMM masses. This is to highlight the combined effect of both corrections in Fig. 1. We first apply this timestamp correction, then Eq. (3).

We denote the resulting temperatures T_{xmm} , with the lowercase indicating that they are converted quantities, not actual *XMM-Newton* measurements. For the eight I14 clusters, whose $\langle T_{\text{CXO}} \rangle = 4.4 \text{ keV}/k_B$ is representative of the full 400d cosmology sample, we measure $\langle T_{\text{xmm}}/T_{\text{CXO}} \rangle = 0.81 \pm 0.01$, using the V09a cluster-averaged temperatures. At r_{500} , measured from weak lensing, the ratio is $\langle T_{\text{xmm}}/T_{\text{CXO}} \rangle = 0.90 \pm 0.01$. This ratio is closer to 1 because $T_X(r_{500})$ is typically lower than $\langle T_X \rangle$ and the cross-calibration differences are smaller for lower T_X according to S14. We ignored the different energy ranges V09a (0.6–10 keV) and S14 (0.7–7 keV) used for fitting spectra.

2.3 Pseudo-XMM-Newton hydrostatic masses

In the next step, we re-derive hydrostatic masses by converting the *Chandra* temperature profiles from Eq. (1) to pseudo-XMM-Newton profiles $T_{\text{xmm}}(r)$. These $T_{\text{xmm}}(r)$ and its value at r_{500} are inserted into Eq. (2), thus accounting for the nonlinear nature of Eq. (3). Because we re-use the same r_{500} estimates as in I14, these apertures do not change. As expected for lower input temperatures and flatter T_X gradients, we find the resulting pseudo-XMM-Newton hydrostatic masses for all clusters to be lower than the *Chandra*-measured values (Fig. 1). The relative difference in masses is strongest for the hottest clusters, for which the S14 conversion results in the largest change. Because the temperatures of the I14 sample exhibit a limited T_X range of 3–6 keV, the relative change of the temperatures varies less than 5 %. Consequently, the two sets of hydrostatic masses are well fit by a linear relation (solid line in Fig. 1):

$$\frac{M_{500}^{\text{xmm}}}{10^{14} M_{\odot}} = P \cdot \frac{M_{500}^{\text{CXO}}}{10^{14} M_{\odot}} + Q \quad (4)$$

with $P = 0.791 \pm 0.030$ and $Q = 0.067 \pm 0.071$ that captures the dependence of the *Chandra*–XMM-Newton disagreement on the measured mass itself. As a sample average and standard error, we find $1 - b_{\text{lin}}^{\text{xcal}} = 1 - \langle M_{500}^{\text{xmm}}/M_{500}^{\text{CXO}} \rangle = 0.82 \pm 0.01$. The difference between this number and the $\langle T_{\text{xmm}}/T_{\text{CXO}} \rangle = 0.90 \pm 0.01$ result can be traced back to the additional factor of $T_X \left(\frac{d \ln T_X(r)}{d \ln r} \right)$ in Eq. (2).

We repeat the experiment without applying the timestamp correction. Doing so, we provide an upper limit for the systematic uncertainty connected to the V09a calibration (see Sect. 2.2). Again comparing to I14 masses, we find $P = 0.837 \pm 0.012$ and $Q = 0.064 \pm 0.024$, and a smaller calibration bias of $1 - b_{\text{lin}}^{\text{xcal}} = 0.86 \pm 0.01$ (dashed line in Fig. 1; Table 1).

Table 1. Observed mass bias in the I14 sample, for several choices of X-ray masses. Columns 2 and 3 give the slope P and intercept Q of the general best-fit relation (Eq. 4) between *Chandra* and *XMM-Newton* masses. Column 4 shows the X-ray calibration bias, i.e. the mean and standard error of $\langle M_{500}^{\text{xmm}} / M_{500}^{\text{CXO},\text{I14}} \rangle$. Columns 5 and 6 show the apparent bias with respect to the I14 WL masses, averaged over jackknifed Monte Carlo simulations for all clusters ($b_{\log} = \langle \log M_{500}^{\text{xmm}} - \log M_{500}^{\text{CXO},\text{I14}} \rangle$) and for the $M_{500}^{\text{wl}} \geq 10^{14.5} \text{ M}_{\odot}$ bin ($b_{\log,\text{H}}$).

Hydrostatic mass	P	Q	$1 - b_{\log}^{\text{xcal}}$	b_{\log}	$b_{\log,\text{H}}$
M_{500}^{CXO} from I14	1	0	1	$0.00^{+0.14}_{-0.13}$	$-0.10^{+0.17}_{-0.15}$
M_{500}^{xmm} , (ACIS-comb. XMM + timestamps)	0.791 ± 0.030	0.067 ± 0.071	0.82 ± 0.01	$-0.08^{+0.15}_{-0.13}$	$-0.20^{+0.17}_{-0.16}$
M_{500}^{xmm} (ACIS-combined XMM)	0.837 ± 0.012	0.064 ± 0.024	0.86 ± 0.01	$-0.06^{+0.15}_{-0.13}$	$-0.17^{+0.17}_{-0.15}$

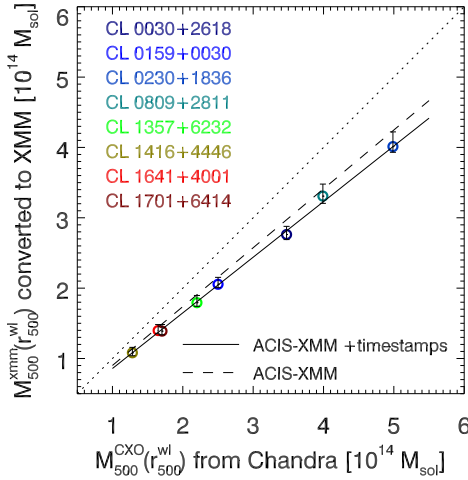


Figure 1. Cluster mass estimates M_{500}^{xmm} derived from pseudo-*XMM-Newton* temperatures and assuming hydrostatic equilibrium as a function of I14 masses M_{500}^{CXO} derived from ICM temperatures observed by *Chandra*. Error bars inscribed in the symbols denote the uncertainty in M_{500}^{xmm} due to the uncertainties in the ACIS-combined XMM and timestamp conversions. Please note that for illustrative purposes, the timestamp correction is not applied to the M_{500}^{CXO} , but its inverse to the M_{500}^{xmm} . The solid line solid line marks the linear best fit. A dashed line marks the best-fit relation when the different *Chandra* calibration timestamps are not taken into account. For the latter case, data points are not shown for the sake of clarity.

2.4 Stronger WL mass bias for pseudo-*XMM-Newton* masses

Figure 2 shows the measured bias between the WL masses M_{500}^{wl} (Israel et al. 2012) and M_{500}^{xmm} (including timestamp correction) for the I14 clusters. The bias is measured by averaging $\langle \log M_{500}^{\text{xmm}} - \log M_{500}^{\text{wl}} \rangle$ over a suite of jackknifed Monte Carlo simulations: As in I14, cluster masses are drawn from their respective probability distributions, modelled as Gaussians described by their 1σ uncertainties. In turn, one cluster out of eight is omitted for 10^5 realisations. This method accounts for correlation between the mass estimates and for extra uncertainty due to the small number of clusters. The results are shown in Table 1 and indicated by a dashed line and shading for the 1σ interval in Fig. 2. Dashed lines and

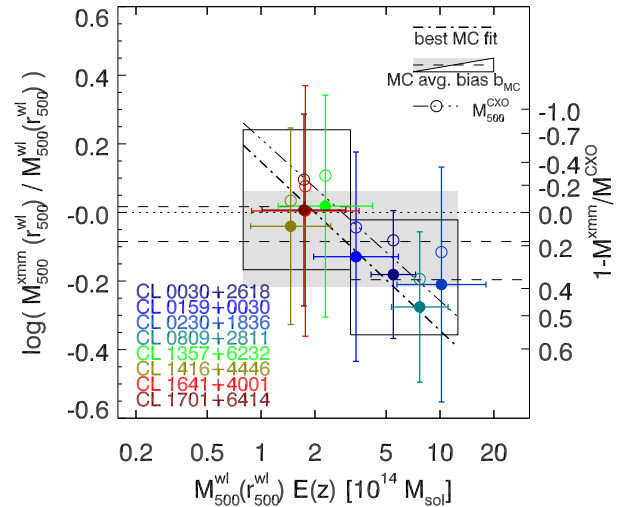


Figure 2. Ratio between the pseudo-*XMM-Newton* hydrostatic mass M_{500}^{xmm} , with timestamp correction, and the I14 WL mass M_{500}^{wl} as a function of M_{500}^{wl} . Short-dashed lines and light grey shading denote the logarithmic bias $b_{\log} = \langle \log M_{500}^{\text{xmm}} - \log M_{500}^{\text{wl}} \rangle$ obtained from averaging over Monte Carlo realisations including the jackknife test. We also show b_{\log} for the low- M^{wl} and high- M^{wl} clusters separately, with the 1σ uncertainties presented as boxes, for sake of clarity. As a visual aid, a dot-dashed line depicts the Monte Carlo/jackknife best-fit of $\log(M_{500}^{\text{xmm}} / M_{500}^{\text{wl}})$ as a function of M^{wl} . Empty symbols and the triple-dot-dashed line denote the M_{500}^{CXO} case from I14. Compare to Fig. 2A in I14.

boxes at $M_{500}^{\text{wl}} \leq 10^{14.5} \text{ M}_{\odot}$ and $M_{500}^{\text{wl}} \geq 10^{14.5} \text{ M}_{\odot}$ show the bias for the thus defined low- and high-mass sub-samples.

For the eight clusters, we now find a pronounced bias of $b_{\log} = -0.08^{+0.15}_{-0.13}$, compared to $b_{\log} = 0.00^{+0.14}_{-0.13}$ from *Chandra* in I14. For the low-mass sub-sample, hydrostatic masses just slightly exceed WL masses ($b_{\log} = 0.02^{+0.22}_{-0.18}$); while for the high-mass sub-sample, we measure $b_{\log} = -0.20^{+0.17}_{-0.16}$, i.e. M_{500}^{xmm} that are smaller than WL masses by a similar amount as the M^{Pl} of vdL14 (cf. Fig. 2).

The mass-dependent bias found in I14 persists, which is unsurprising given the small sample size and narrow T_X range. Its likely cause is a combination of physical effects, e.g., stronger hydrostatic bias for high-mass clusters (Shi & Komatsu 2014) or different physical processes at work in low-mass clusters (I14), and Eddington bias. As Sereno &

Ettori (2014) demonstrate, intrinsic scatter in the abscissa mass leads to a mass-dependent bias when compared to an independent mass observable.

We repeat our analysis excluding the *Chandra* timestamp variations (Sect. 2.3) and arrive at a lower apparent bias compared to including them: $b_{\log} = -0.06^{+0.15}_{-0.13}$ (Table 1). The difference between those two cases may serve as an estimate for the systematic uncertainties in the observatory conversions.

Considering the full mass range, the *XMM-Newton* hydrostatic masses are ~ 20 % lower than the WL masses, while *Chandra* masses are consistent with the WL masses. This indicates that if the $b_{\text{lin}} = 0.2$ linear hydrostatic bias in cluster simulations is correct, the effective area calibration of *XMM-Newton* is consistent with being correct. But if looking at the high mass end, the conclusion is the opposite: *Chandra* is consistent with the correct calibration and 20 % hydro bias. The measurement uncertainties and the unknown amount of Eddington bias in our small sample, however, preclude more quantitative conclusions.

3 TRANSLATION TO PLANCK CLUSTERS

3.1 Comparison to *Planck* and vdl14 samples

The mean WL mass of the I14 clusters is $3.2 \cdot 10^{14} \text{ M}_{\odot}$, while the mean WL mass of the high-mass sub-sample is $4.9 \cdot 10^{14} \text{ M}_{\odot}$. The typical P13XX cluster mass, defined by their mass pivot $\sim 6 \cdot 10^{14} \text{ M}_{\odot}$, falls into the mass range probed by the I14 high- M^{wl} range, even although the mass bias is not included. Therefore, for the relevant P13XX mass range, our result of $b_{\log, \text{H}} = 0.20^{+0.17}_{-0.16}$ agrees with the $1 - b_{\text{lin}} \approx 0.4$ that would reconcile cosmological constraints derived from *Planck* cluster counts (P13XX) and primary CMB anisotropies (P13XVI).

The high-mass end of the I14 sample also overlaps with the vdl14 sample. Using the M_{500}^{xmm} for the I14 clusters instead of *Chandra* masses, we also find better agreement to the vdl14 measurement of $\langle M^{\text{Pl}}/M^{\text{wl}} \rangle = 0.688 \pm 0.072$ for a subset of P13XX clusters. However, such comparisons are limited by the small number statistics of our sample, hence caution is necessary when interpreting these results.²

A first complication is that it has not been made public which *XMM-Newton* instruments were considered in the P13XXIX calibration. Another complication arises from the temporal variability of X-ray calibrations. Our results for the cases with and without timestamp correction (Table 1) tell us, however, that the impact of those systematics is rather small, with $\Delta b_{\text{lin}} \lesssim 0.05$.

3.2 How much can X-ray calibration bias have influenced the P13XX results?

We attempt to estimate how an additional bias $b_{\text{lin}}^{\text{xcal}}$ arising from the *XMM-Newton* calibration relative to *Chandra* will

² The difference in cosmologies between P13XX and vdl14 on the one hand (flat universe with matter density $\Omega_m = 0.3$ and Hubble parameter $H_0 = 70 \text{ km s}^{-1} \text{ Mpc}^{-1}$) and I14 and this work on the other hand (the same, but $H_0 = 72 \text{ km s}^{-1} \text{ Mpc}^{-1}$) adds a factor of 70/72 to convert *Planck* masses to our cosmology.

influence the overall bias measured by P13XX. We emphasise that we do not know or assume which, if any, satellite calibration is correct. The “pre-calibration” from 20 relaxed clusters (Arnaud et al. 2010) determines the normalisation 10^B and slope β of a scaling relation

$$E^{-2/3}(z) \left[\frac{Y_X}{2 \cdot 10^{14} \text{ M}_{\odot} \text{ keV}} \right] = 10^B \cdot \left[\frac{M_{500}^{\text{HE}}}{6 \cdot 10^{14} \text{ M}_{\odot}} \right]^{\beta} \quad (5)$$

between the Y_X and hydrostatic masses M_{500}^{HE} measured with *XMM-Newton*. The evolution factor $E(z) = H(z)/H(z=0)$ depends on cosmology via the Hubble parameter $H(z)$.

In Eq. (5), M_{500}^{HE} scales roughly as $T_X^{3/2}$ (e.g., Kay et al. 2012), through the measurement at r_{500} . If $q = T_{\text{XMM}}/T_{\text{CXO}}$ for the typical Arnaud et al. (2010) cluster, hydrostatic masses are biased $M_{500}^{\text{HE}} \rightarrow q^{\delta} M_{500}^{\text{HE}}$, with $\delta \approx 1.5$. Similarly, Y_X depends on T_X via the measurement of the gas mass M_{gas} within r_{500} : We have $r_{500} \propto M_{500}^{1/3}$. If $M_{500} \propto T_X^{3/2}$ upon a change in T_X , then $r_{500} \propto (T_X^{3/2})^{1/3} = T_X^{1/2}$. Because $M_{\text{gas}}(< r)$ increases linearly with r in a given cluster³ it follows $M_{\text{gas},500} \propto T_X^{1/2}$ upon a change in T_X . Indeed, we measure $M_{\text{gas},500}$ to be affected as $q^{0.5}$ to $q^{0.6}$ by a relative temperature change q , using the V09a gas density model for the I14 clusters. Hence, we have $Y_X \rightarrow q^{\gamma} Y_X$ with an exponent $\gamma \approx 1.5$.

We assume we can use the temperature ratio q at a typical T_{XMM} and ignore its T_{XMM} dependence.⁴ Then, the temperature calibrations affects Eq. (5) like:

$$q^{\gamma} Y_X \propto [q^{\delta} M_{500}^{\text{HE}}]^{\beta} \Leftrightarrow Y_X \propto q^{\beta\delta-\gamma} [M_{500}^{\text{HE}}]^{\beta}. \quad (6)$$

This means that for a (residual, unaccounted) temperature bias q , the mass proxy $M_{500}^{Y_X}$ will be biased by a factor $q^{\beta\delta-\gamma}$. The main P13XX scaling relation

$$E^{-2/3}(z) \left[\frac{D_A^2 Y_{\text{SZ},500}}{10^{-4} \text{ Mpc}^2} \right] = 10^A \cdot \left[\frac{M_{500}^{Y_X}}{6 \cdot 10^{14} \text{ M}_{\odot}} \right]^{\alpha} \quad (7)$$

relates the masses $M_{500}^{Y_X}$ to Y_{500} instead of Y_X , with D_A denoting the angular diameter distance. However, Y_X is theoretically expected to be proportional to Y_{SZ} , so we can identify $\alpha = \beta$ and find a modified Eq. (7):

$$E^{-2/3}(z) \left[\frac{D_A^2 Y_{\text{SZ},500}}{10^{-4} \text{ Mpc}^2} \right] = 10^A q^{\alpha\delta-\gamma} \cdot \left[\frac{M_{500}^{Y_X}}{6 \cdot 10^{14} \text{ M}_{\odot}} \right]^{\alpha}. \quad (8)$$

Given a bias factor q in the ICM temperatures, the calibration scaling relation will be offset by a factor $C = q^{\alpha\delta-\gamma}$.

The properties of the local, relaxed galaxy clusters from which Arnaud et al. (2010) calibrated Eq. (5) are given in Arnaud, Pointecouteau & Pratt (2007); Pratt et al. (2010). We measure an average $k_B T_{\text{XMM}} \approx 5 \pm 2 \text{ keV}$ for the clusters implicated to constitute the calibration sample. Following Eq. (3), the S14 conversion for the combined *XMM-Newton* instruments, *Chandra* temperatures for these clusters would be lower by a factor of $q = 0.84^{+0.05}_{-0.03}$. With $\alpha = 1.79$

³ If the cluster is isothermal, and $\rho_{\text{gas}} \propto r^{-2}$, as motivated by assuming the standard $\beta = 2/3$ in the β model for the gas density (Cavaliere & Fusco-Femiano 1978), then the 3D mass within a radius R is $M(< R) = \int_0^R \rho_{\text{gas}}(r) dV \propto \int_0^R r^{-2} r^2 dr = R$.

⁴ In principle, the T_{XMM} -dependence should be considered. This would alter the slope β in Eq. (5). While making an interesting point, this would complicate this consideration of an extreme case.

from P13XX, $\gamma = 3/2$, and $\delta = 3/2$ (see above), we find the normalisation of Eq. (7) to be reduced by a factor of $C = q^{1.185} = 0.81_{-0.03}^{+0.06}$. If we allow for broad uncertainties $1.3 < \gamma, \delta < 1.8$, a temperature bias q will propagate as $C \approx q^{0.5}$ to $C \approx q^{2.0}$ in the extreme cases.

The exact algorithm by which P13XXIX combine *Planck* measurements with Eq. (7) has yet to be published. However, using $\theta_{500} = (3M_{500}/[4\pi\rho_c D_A^3])^{1/3}$, one can easily convert Eq. (7) into a scaling relation in terms of an aperture scale θ_{500} , i.e.: $Y_{\text{SZ}} \propto \theta_{500}^{3\alpha}$. The intersection of this relation with the size–flux degeneracy modelled as $Y_{\text{SZ}}^{\text{obs}} \propto \theta^\lambda$ yields a point (θ_x, Y_x) , that can in turn be used to compute an SZ mass $M_{\text{Pl}} \propto \theta_x^3$. Thus, the degeneracy is broken. How is this M_{Pl} affected if the normalisation of Eq. (7) changes by a factor C ? We geometrically infer the changes in the intersection point and final mass as:

$$\log(Y'_x/Y_x) = [-\lambda/(\lambda-3\alpha)] \cdot \log C \quad (9)$$

$$\log C_{\text{fin}} = \log(M'_{\text{Pl}}/M_{\text{Pl}}) = [-3\alpha\lambda/(\lambda-3\alpha)] \cdot \log C. \quad (10)$$

From Fig. 4 of P13XXIX, we read that the $Y_{\text{SZ}}^{\text{obs}} - \theta$ relation is linear, so $\lambda = 1$. With $C = 0.81_{-0.03}^{+0.05}$ from above, we find that cluster masses would be biased low by a factor $C_{\text{fin}} = 0.78_{-0.04}^{+0.07}$ due to the temperature calibration. Thus, if the *Chandra* calibration was correct, the need for a hydrostatic mass bias of more than the $\sim 20\%$ favoured by simulations would be eased. Alternatively, if the *XMM-Newton* calibration was correct, evidence for stronger departures from hydrostatic equilibrium would persist.

We note that the “hydrostatic” bias b_{lin} that P13XX consider is meant to include instrument calibration effects: $1-b_{\text{lin}} = (1-b_{\text{lin}}^{\text{hyd}})(1-b_{\text{lin}}^{\text{xcal}}) \approx (1-b_{\text{lin}}^{\text{hyd}} - b_{\text{lin}}^{\text{xcal}})$. Nevertheless even a partially unaccounted calibration bias would contribute some of the apparent mass discrepancy. The point of this exercise lies not in suggesting that the *Planck* discrepancy is caused by the X-ray calibration. Rather it should serve to demonstrate how such effects can not only fold through but even become amplified in a multi-step calibration.

3.3 Summary and Outlook

Starting from the recent Schellenberger et al. (2014) comparative study of ICM temperatures measured with *Chandra* and *XMM-Newton*, we revisit the bias between WL and hydrostatic masses from Israel et al. (2014). We find:

1. Because of different uncertainties in the effective area calibration, hydrostatic masses for the I14 clusters would have been measured to be $\sim 15\text{--}20\%$ lower, had the clusters been observed with *XMM-Newton* instead of *Chandra*. The measured calibration bias depends on the sample, but can be transferred to clusters of similar mass ($10^{14}\text{--}10^{15} M_\odot$).

2. *XMM-Newton* masses for the most massive I14 clusters are lower than WL masses by $\sim 35\%$.

3. Assuming a true hydrostatic bias of $b_{\text{lin}}^{\text{hyd}} = 0.2$, our results for the whole mass range indicate that the calibration of the energy dependence of the effective area of the *XMM-Newton* EPIC instruments in the 0.6–10.0 keV band is rather accurate. In the high mass range the data however indicate that *Chandra* calibration is more accurate. Given the uncertainties these results are not significant.

In addition, we consider the *Planck* clusters and find:

4. Hence, consistent with vdl14, a bias of $(1-b_{\text{lin}}^{\text{hyd}} - b_{\text{lin}}^{\text{xcal}}) \approx 0.4$ for the rather massive P13XX clusters seems plausible.

5. If there was a residual calibration bias q in the T_{XMM} measurements on which the *Planck* analysis is based, the normalisation of the P13XX $Y_{\text{SZ}} - M^{\text{YX}}$ calibration would be affected as $C = q^{\sim 1.2}$.

6. Using a simple model for how this normalisation affects SZ masses, we show how the mass bias can be further amplified. Without account for calibration uncertainties, a mass bias of up to 30 % is plausible. We do not claim that this is the case for *Planck*. However, a small, residual bias would amplify in the same way. Pointing to the S14 result that calibration alone cannot explain the discrepant cosmological parameters of P13XVI and P13XXIX, we conclude that a possible contribution would ease the discrepancy and allow for a true hydrostatic bias consistent with simulations.

Our results are consistent with the WL/X-ray mass biases recently reported by Donahue et al. (2014), comparing CLASH WL mass profiles to those obtained with *Chandra* and *XMM-Newton*. Donahue et al. (2014) found their $T_{\text{XMM}}/T_{\text{CXO}}$ and $M^{\text{XMM}}/M^{\text{WL}}$ to depend on the integration radius; suggesting soft X-ray scattering as a cause for the calibration offset. Donahue et al. (2014) study mostly cool core clusters. Since S14 find that the T_x bias depends on T_x , this could explain why they find less bias in the cooler centres. The radial dependence could at least partly be due to a secondary correlation: at the radius where the cluster temperature is typically hottest, the largest discrepancy between *Chandra* and *XMM-Newton* is found.

Cluster mass calibrations still bear considerable uncertainties not only between the main techniques (X-ray, lensing, SZ, galaxy-based), but also within techniques, i.e. for different instruments and calibration and methods. Thorough cross-calibration of different instruments and techniques, as already performed by Nevalainen, David & Guainazzi (2010); Schellenberger et al. (2014); Rozo et al. (2014b,a) for X-rays are the necessary way forward. Recent comparisons of WL masses to both *XMM-Newton* and *Chandra* include Mahdavi et al. (2013); Donahue et al. (2014), and Martino et al. (2014). We notice that Martino et al. (2014) find temperature discrepancies between *XMM-Newton* and *Chandra* similar to S14, but consistent hydrostatic masses from both satellites. More overlap between clusters with X-ray and WL data would be necessary to define mass standards against which other surveys could then be gauged.

Recently, Sereno & Ettori (2014); Sereno, Ettori & Moscardini (2014) compared several of the larger current WL and *XMM-Newton* and *Chandra* X-ray samples, emphasising how intrinsic and measurement scatter can induce scaling relation biases. Sereno & Ettori (2014) confirm that compared to simulated clusters WL masses are biased low by $\sim 10\%$ and hydrostatic masses by $\sim 20\text{--}30\%$. However, these authors find literature masses *from the same observable*, X-ray or WL, can differ up to 40 % for the same cluster, impeding an absolute calibration. Sereno, Ettori & Moscardini (2014) extend the analysis to the *Planck* clusters, whose absolute mass calibration is likewise affected. They find scatter in the calibration scaling relation to invoke a mass-dependent bias in the *Planck* masses.

The advent of larger SZ samples for scaling relation studies (e.g., Bender et al. 2014; Czakon et al. 2014; Liu

et al. 2014), and foremost the all-sky P13XXIX offers the possibility to include a complementary probe and clusters at higher redshift. For future high precision cluster experiments, e.g., *eROSITA* (Predehl et al. 2010; Merloni et al. 2012; Pillepich, Porciani & Reiprich 2012) or *Euclid* (Lau-reijs et al. 2011; Amendola et al. 2012) the absolute X-ray observable–mass calibration needs to be improved further.

REFERENCES

Amendola L. et al., 2012, ArXiv astro-ph.CO/1206.1225
 Applegate D. E. et al., 2014, MNRAS, 439, 48
 Arnaud M., Pointecouteau E., Pratt G. W., 2007, A&A, 474, L37
 Arnaud M., Pratt G. W., Piffaretti R., Böhringer H., Croston J. H., Pointecouteau E., 2010, A&A, 517, A92
 Batty R. A., Moss A., 2014, Physical Review Letters, 112, 051303
 Bender A. N. et al., 2014, ArXiv astro-ph.CO/1404.7103
 Bhattacharya S., Habib S., Heitmann K., Vikhlinin A., 2013, ApJ, 766, 32
 Burenin R. A., Vikhlinin A., Hornstrup A., Ebeling H., Quintana H., Mescheryakov A., 2007, ApJS, 172, 561
 Cavaliere A., Fusco-Femiano R., 1978, A&A, 70, 677
 Costanzi M., Sartoris B., Viel M., Borgani S., 2014, ArXiv astro-ph.CO/1407.8338
 Czakon N. G. et al., 2014, ArXiv astro-ph.CO/1406.2800
 Donahue M. et al., 2014, ArXiv astro-ph.CO/1405.7876
 Grant C. E., Guainazzi M., Natalucci L., Nevalainen J., Plucinsky P. P., Pollock A., Sembay S., 2013, ArXiv astro-ph.IM/1305.4480
 Hamann J., Hasenkamp J., 2013, JCAP, 10, 44
 Israel H. et al., 2010, A&A, 520, A58
 Israel H., Erben T., Reiprich T. H., Vikhlinin A., Sarazin C. L., Schneider P., 2012, A&A, 546, A79
 Israel H., Reiprich T. H., Erben T., Massey R. J., Sarazin C. L., Schneider P., Vikhlinin A., 2014, A&A, 564, A129
 Kay S. T., Peel M. W., Short C. J., Thomas P. A., Young O. E., Batty R. A., Liddle A. R., Pearce F. R., 2012, MNRAS, 422, 1999
 Kelly P. L. et al., 2014, MNRAS, 439, 28
 Laganá T. F., de Souza R. S., Keller G. R., 2010, A&A, 510, A76
 Laureijs R. et al., 2011, ArXiv astro-ph.CO/1110.3193
 Le Brun A. M. C., McCarthy I. G., Schaye J., Ponman T. J., 2014, MNRAS, 441, 1270
 Liu J. et al., 2014, ArXiv astro-ph.CO/1407.7520
 Mahdavi A., Hoekstra H., Babul A., Bildfell C., Jeltema T., Henry J. P., 2013, ApJ, 767, 116
 Mantz A. B. et al., 2014, ArXiv astro-ph.CO/1407.4516
 Martino R., Mazzotta P., Bourdin H., Smith G. P., Bartalucci I., Marrone D. P., Finoguenov A., Okabe N., 2014, ArXiv astro-ph.CO/1406.6831
 Merloni A. et al., 2012, ArXiv astro-ph.HE/1209.3114
 Nagai D., Kravtsov A. V., Vikhlinin A., 2007, ApJ, 668, 1
 Nevalainen J., David L., Guainazzi M., 2010, A&A, 523, A22
 Pillepich A., Porciani C., Reiprich T. H., 2012, MNRAS, 422, 44
 Planck Collaboration et al., 2013a, ArXiv astro-ph.CO/1303.5089
 Planck Collaboration et al., 2013b, ArXiv astro-ph.CO/1303.5076
 Planck Collaboration et al., 2013c, ArXiv astro-ph.CO/1303.5080
 Pratt G. W. et al., 2010, A&A, 511, A85
 Predehl P. et al., 2010, in Society of Photo-Optical Instrumentation Engineers (SPIE) Conference Series, Vol. 7732
 Rasia E. et al., 2012, New Journal of Physics, 14, 055018
 Reese E. D., Kawahara H., Kitayama T., Ota N., Sasaki S., Suto Y., 2010, ApJ, 721, 653
 Reiprich T. H., Basu K., Ettori S., Israel H., Lovisari L., Molendi S., Pointecouteau E., Roncarelli M., 2013, Space Sci. Rev., 195
 Rozo E., Evrard A. E., Rykoff E. S., Bartlett J. G., 2014a, MNRAS, 438, 62
 Rozo E., Rykoff E. S., Bartlett J. G., Evrard A., 2014b, MNRAS, 438, 49
 Schaye J. et al., 2014, ArXiv astro-ph.GA/1407.7040
 Schellenberger G., Reiprich T. H., Lovisari L., Nevalainen J., David L., 2014, ArXiv astro-ph.IM/1404.7130
 Sereno M., Ettori S., 2014, ArXiv astro-ph.CO/1407.7868
 Sereno M., Ettori S., Moscardini L., 2014, ArXiv astro-ph.CO/1407.7869
 Shi X., Komatsu E., 2014, MNRAS, 442, 521
 Vikhlinin A. et al., 2009a, ApJ, 692, 1033
 Vikhlinin A., Kravtsov A., Forman W., Jones C., Markevitch M., Murray S. S., Van Speybroeck L., 2006, ApJ, 640, 691
 Vikhlinin A. et al., 2009b, ApJ, 692, 1060
 Vikhlinin A., Markevitch M., Murray S. S., Jones C., Forman W., Van Speybroeck L., 2005, ApJ, 628, 655
 von der Linden A. et al., 2014a, MNRAS, 439, 2
 von der Linden A. et al., 2014b, MNRAS, 443, 1973

ACKNOWLEDGEMENTS

HI likes to thank D. Applegate for a helpful discussion. HI acknowledges support through European Research Council grant MIRG-CT-208994. JN acknowledges a PUT 246 grant from Estonian Research Council. RJM is supported by a Royal Society University Research Fellowship and Philip Leverhulme Prize PLP-2011-003. THR acknowledges support from the German Research Association (DFG) through Heisenberg grant RE 1462/5 and through the Transregional Collaborative Research Centre TRR33 “The Dark Universe” (project B18). GS and THR acknowledge DFG grant RE 1462/6.